Electronic Supplementary Information (ESI)

Spin crossover cobalt(II) complexes exhibiting temperature- and concentration-dependent optical changes in solution

Naoki Izumiyama,[a] Shun Fujii,[a] Kiichi Kato,[b] Ryuya Tokunaga,[c] Shinya Hayami[c,d] and Manabu Nakaya*[a,b]

[a]Department of Material Science, Graduate School of Science, Josai University, 1-1 Keyakidai, Sakado, Saitama 350-0295, Japan.

[b]Department of Chemistry, Faculty of Science, Josai University, 1-1 Keyakidai, Sakado, Saitama 350-0295, Japan.

[c]Department of Chemistry, Graduate School of Science and Technology, Kumamoto University, 2-39-1 Kurokami, Chuo-ku, Kumamoto 860-8555, Japan.

[d]Institute of Industrial Nanomaterials (IINa), Kumamoto University, 2-39-1 Kurokami, Chuo-ku, Kumamoto 860-8555, Japan

EXPERIMENTAL SECTION

Synthesis. All reagents were commercially available and used without further purification.

*Synthesis of 4'-(4-N,N'-diphenylaminophenyl)-2,2':6',2''-terpyridine (**L1**).* 4-(N,N-diphenyl amino)benzaldehyde (2.733 g, 10 mmol) and excess amount of 2-Acetylpyridine (24.23 g, 200 mmol) were stirred in ethanol (150 mL) at room temperature. To the solution was added KOH (11.22 g, 200 mmol) and NH_4aq. (57 mL) and stirred at room temperature for further 12 hours. The color of the solution changed from yellow to red and a yellow precipitate gradually formed. The precipitate was then collected by filtration, washed with water and ethanol, and dried in vacuum to give **L1** (2.912 g, 61 % yield). ^{1}H-NMR (400 MHz, $CDCl_3$): δ = 8.73-8.71 (m, 4H), 8.68-8.65 (m, 2H), 7.90-7.85 (m, 2H), 7.80-7.78 (m, 2H), 7.36-7.33 (m, 2H), 7.32-7.27 (m, 4H), 7.19-7.14 (m, 6H), 7.09-7.05 (m, 2H) ppm.

*Synthesis of 4'-(4-N,N'-dimethylaminophenyl)-2,2':6',2''-terpyridine (**L2**).* 4-dimethylaminobenzaldehyde (1.490 g, 10 mmol) and 2-acetylpyridine (2.433 g, 20 mmol) were stirred in ethanol (50 mL) at room temperature. To the solution was added KOH (1.155 g, 20 mmol) and NH_4aq. (17 mL) and stirred at room temperature for 12 hours. The color of the solution changed from yellow to red and finally a yellowish precipitate formed. The precipitate was then collected by filtration, washed with water and ethanol, and dried in vacuum to give **L2** (1.055 g, 30 % yield). ^{1}H-NMR (400 MHz, $CDCl_3$): δ = 8.74-8.72 (m, 2H), 8.71 (s, 2H), 8.67-8.65 (m, 2H), 7.89-7.84 (m, 4H), 7.35-7.32 (m, 2H), 6.83-6.81 (m, 2H), 3.05 (s, 6H) ppm.

*Synthesis of complex **1·X**.* A quantity of **L1** (0.509 g, 1.45 mmol) was dissolved in $CHCl_3$ (40 mL) after which a solution of $CoCl_2 \cdot 6H_2O$ (0.172 g, 0.723 mmol) in MeOH (40 mL) was added dropwise to the solution. The solution immediately turned to dark red color. The solution was then stirred for further 2 h at room temperature. To this solution was added a saturated methanol solution of KPF_6 for **1·PF$_6$** and $NaBPh_4$ for **1·BPh$_4$**, respectively. The precipitate was collected by filtration and washed with a small amount of MeOH to give **1·PF$_6$** (27.0%) and **1·BPh$_4$** (60.1%). Calcd. for **1·PF$_6$·3MeOH**: H 3.93, C 60.32, N 8.40.; Found: H 3.95, C 60.51, N 8.60. Calcd. for **1·BPh$_4$·2.5H$_2$O**: H 5.53, C 80.75, N 6.61., Found: H 5.58, C 80.68, N 6.81.

*Synthesis of complex **2·X**.* A quantity of **L2** (0.420 g, 1.19 mmol) was dissolved in $CHCl_3$ (40 mL) after which a solution of $CoCl_2 \cdot 6H_2O$ (0.142 g, 0.595 mmol) in MeOH (40 mL) was added dropwise to the solution. The solution immediately turned to dark red color. The solution was then stirred for further 2 h at room temperature. To this solution was added a saturated methanol solution of KPF_6 for **2·PF$_6$** and $NaBPh_4$ for **2·BPh$_4$**, respectively. The precipitate was collected by filtration and washed with a small amount of MeOH to give **2·PF$_6$** (42.2%) and **2·BPh$_4$** (30.0%). Elemental analysis: Calcd. for **2·PF$_6$·2.5H$_2$O**: H 4.13, C 50.28, N 10.20.; Found: H 4.11, C 50.22, N 10.12. Calcd. for **2·BPh$_4$·1.5MeOH**: H 5.98, C 79.09, N 7.73., Found: H 5.85, C 78.97, N 7.72.

Physical measurements. ^{1}H-NMR spectra were acquired with a Bruker AVANCE NEO 400 instrument operating at 400 MHz, using the deuterated solvent to provide the lock signal and residual solvent tetramethylsilane as the internal reference. Elemental analyses for C, H and N were carried out at the Instrumental Analysis Centre of Josai University. SC-XRD measurements were recorded on an Oxford Gemini Ultra diffractometer employing graphite monochromated Mo Kα radiation generated from a sealed tube (λ = 0.7107 Å). Data integration and reduction were undertaken with APEX4 program. The structures were solved by Olex2 with the ShelXT structure solution program using Direct Methods and refined with the ShelXL refinement package using Least Squares minimization. Hydrogen atoms were included in idealized positions and refined using a riding model.

Magnetic susceptibilities were measured with a superconducting quantum interference device (SQUID) magnetometer (Quantum Design MPMS-XL). Samples were put into a gelatin capsule, mounted in-side a straw, and then fixed to the end of the sample transport rod. Cooperativity was estimated from the measured $\chi_m T$ versus T curves (χ_m; molar magnetic susceptibility, T; temperature) by applying the regular solution model (eq. 1), where ΔH, ΔS and Γ are the enthalpy and the entropy variations and the parameter accounting for cooperativity based on SCO, respectively. The HS molar fraction, γ_{HS}, is shown as a function of the magnetic susceptibility via (eq. 2), where $(\chi_m T)_m$ is the $\chi_m T$ value at any temperature, $(\chi_m T)_{HS}$ and $(\chi_m T)_{LS}$ are the pure LS and HS states, respectively. R is the gas constant unit, 8.314 J K^{-1} mol^{-1}. The cooperativity value, C, is given by eq. 3.

$$\ln[(1-\gamma_{HS})/(\gamma_{HS})] = [\{\Delta H+\Gamma(1-2\gamma_{HS})\}/RT]-\Delta S/R \qquad \text{(eq. 1)}$$

$$\gamma_{HS} = [(\chi_m T)_m-(\chi_m T)_{LS}]/[(\chi_m T)_{HS}-(\chi_m T)_{LS}] \qquad \text{(eq. 2)}$$

$$C = \Gamma/(2RT_{1/2}),\ T_{1/2} = \Delta H/\Delta S \qquad \text{(eq. 3)}$$

Table S1 Crystal parameters for **1·X** and **2·X** (X = PF_6 and BPh_4).

	1·PF_6·2CH_3CN	**1·BPh_4·solv**	**2·PF_6**	**2·BPh_4**
CCDC number	2332745	2332743	2332744	2332746
Formula	$C_{70}H_{53}CoF_{12}N_{10}P_2$	$C_{120.30}H_{99.45}B_2CoN_{10.75}O_{1.05}$	$C_{92}H_{80}Co_2F_{24}N_{16}P_4$	$C_{94}H_{80}B_2CoN_8$
T/K	100	100	100	100
Crystal system	monoclinic	triclinic	triclinic	orthorhombic
Space group	*P*2$_1$/*c*	*P*-1	*P*-1	*Pna*2$_1$
a / Å	10.5636(4)	15.9874(6)	15.346(2)	39.4872(17)
b / Å	16.2032(6)	18.4762(8)	16.020(2)	11.4740(4)
c / Å	35.9590(17)	19.2522(8)	18.525(3)	16.3188(8)
α / °	90	98.6460(10)	75.417(5)	90
β / °	91.231(2)	112.5360(10)	89.684(5)	90
γ / °	90	105.9460(10)	88.213(6)	90
V / Å^3	6153.5(4)	4836.7(3)	4405.6(11)	7393.7(5)
Z	4	2	2	4
GOF	1.023	1.032	1.068	1.073
R1	0.0604	0.0461	0.1285	0.0462
wR2	0.1668	0.1248	0.3185	0.1042

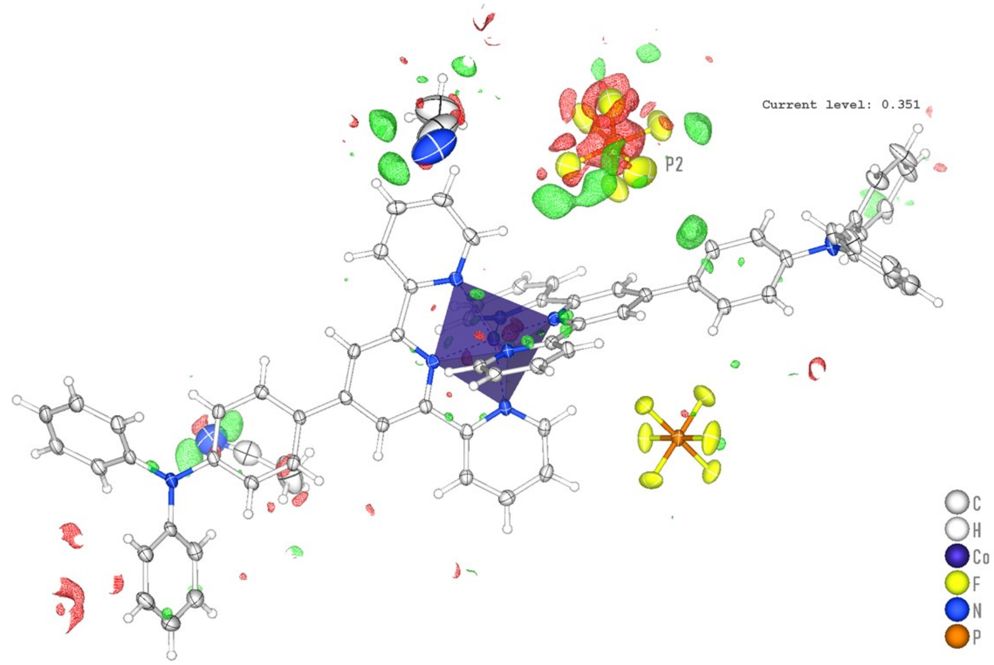

Fig. S1 Residual density plots for **1·PF$_6$·2CH$_3$CN**. PF$_6^-$ anion (displayed as P2) is about 85:15 disordered (The occupancy was set as 100 % here to avoid the misleading for the stoichiometric ratio).

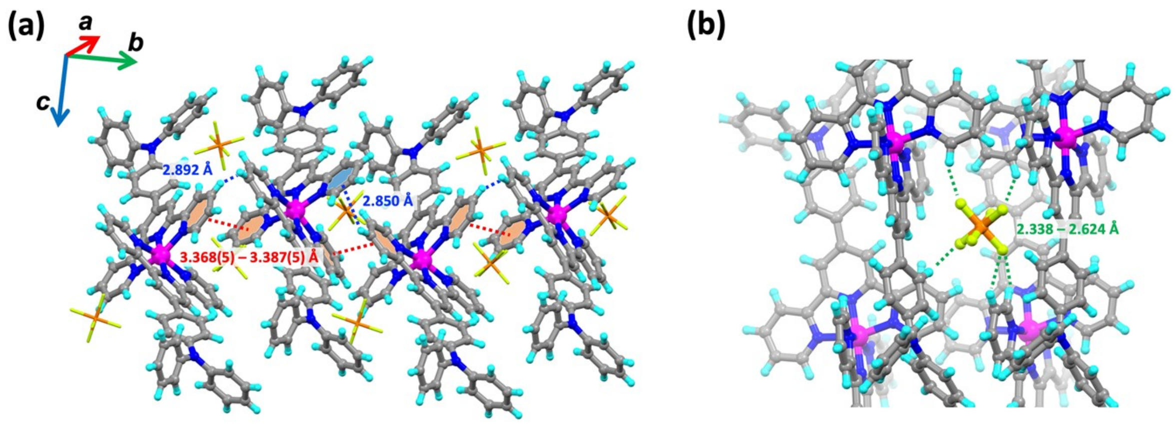

Fig. S2 The selected intermolecular interactions observed in the molecular assembly of **1·PF$_6$·2CH$_3$CN**. (a) Illustration of intermolecular π–π interactions (red dashed line) and CH–π interactions (blue dashed line), respectively. (b) Intermolecular hydrogen bond between [Co(**L1**)]$^{2+}$ units and PF$_6^-$ counter anion (green dashed line).

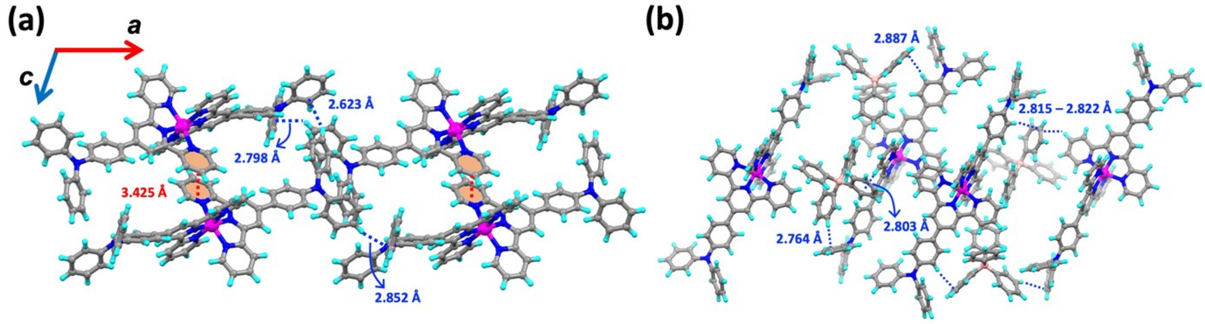

Fig. S3 The selected intermolecular interactions observed in the molecular assembly of **1·BPh$_4$·solv**. (a) Illustration of intermolecular π–π interactions (red dashed line) and CH–π interactions (blue dashed line), respectively, among the [Co(**L1**)]$^{2+}$ units. BPh_4^- counter anions are omitted for clarity. (b) Intermolecular hydrogen bonds between [Co(**L1**)]$^{2+}$ units and BPh_4^- counter anion (green dashed line).

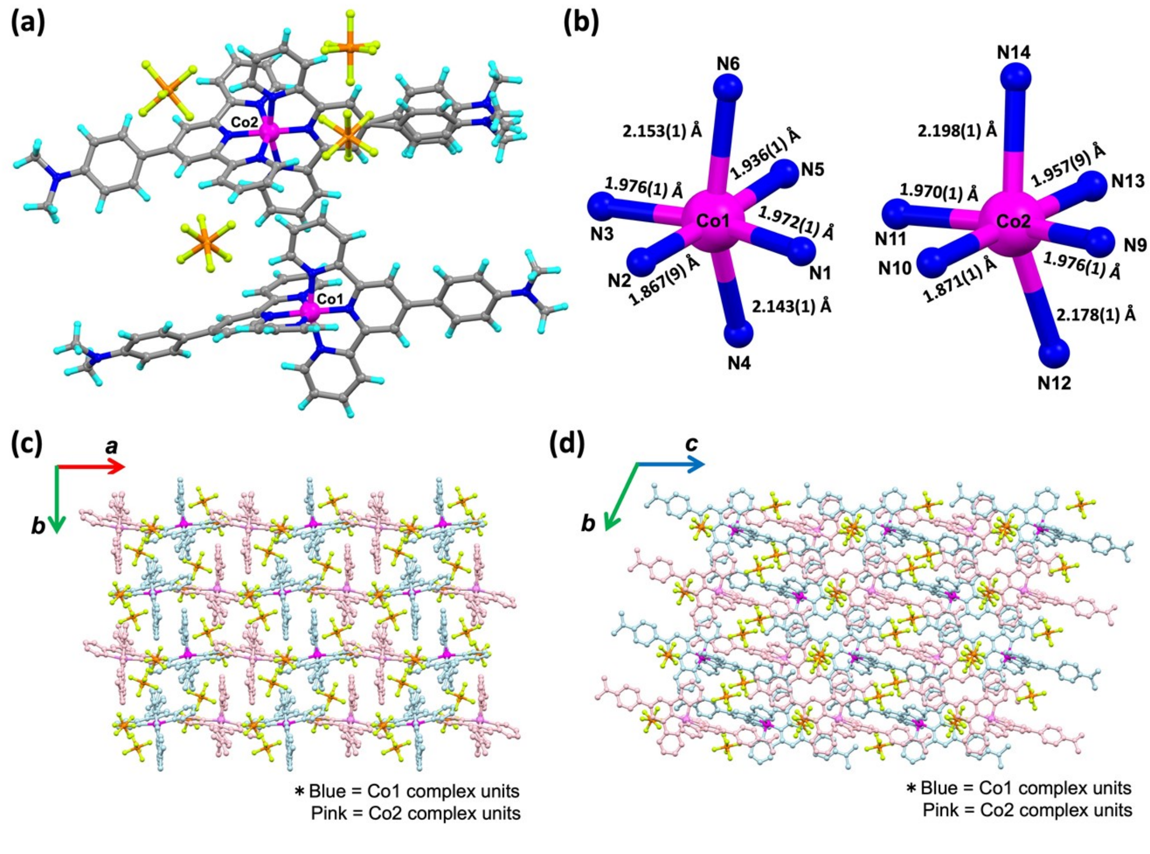

Fig. S4 (a) Crystal structure of **2·PF$_6$**. One diphenylamine site which of Co2 complex was located with disorder. (b) Coordination environment of the [CoN6] core and the Co–N bond length. Crystal packing of **2·PF$_6$** along (c) the *ab* plane and (d) the *bc* plane. Blue and pink coloured molecules are [Co(**L2**)$_2$]$^{2+}$ cations consisting of Co1 and Co2 metal center, respectively.

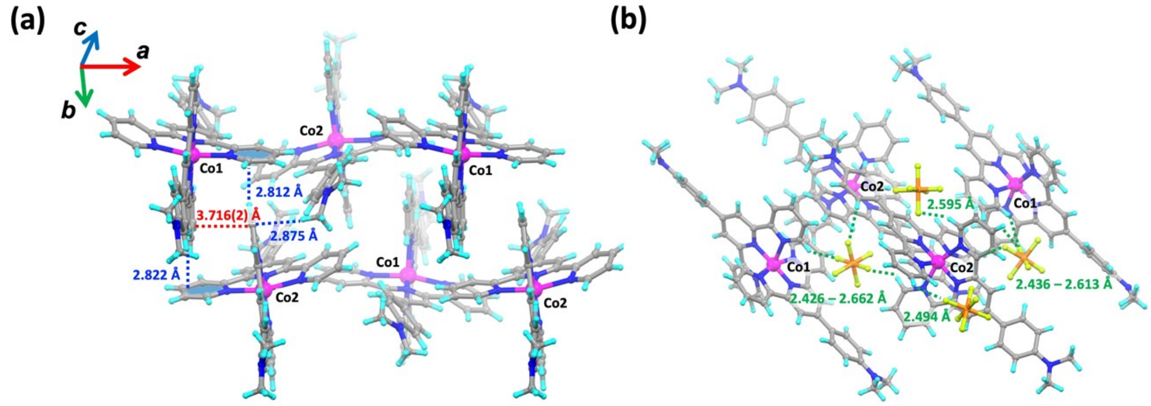

Fig. S5 The selected intermolecular interactions observed in the molecular assembly of **2·PF$_6$**. (a) Illustration of intermolecular π–π interactions (red dashed line) and CH–π interactions (blue dashed line), respectively, among the [Co(**L2**)]$^{2+}$ units. PF_6^- counter anions are omitted for clarity. (b) Intermolecular hydrogen bond between [Co(**L2**)]$^{2+}$ units and PF_6^- counter anion (green dashed line).

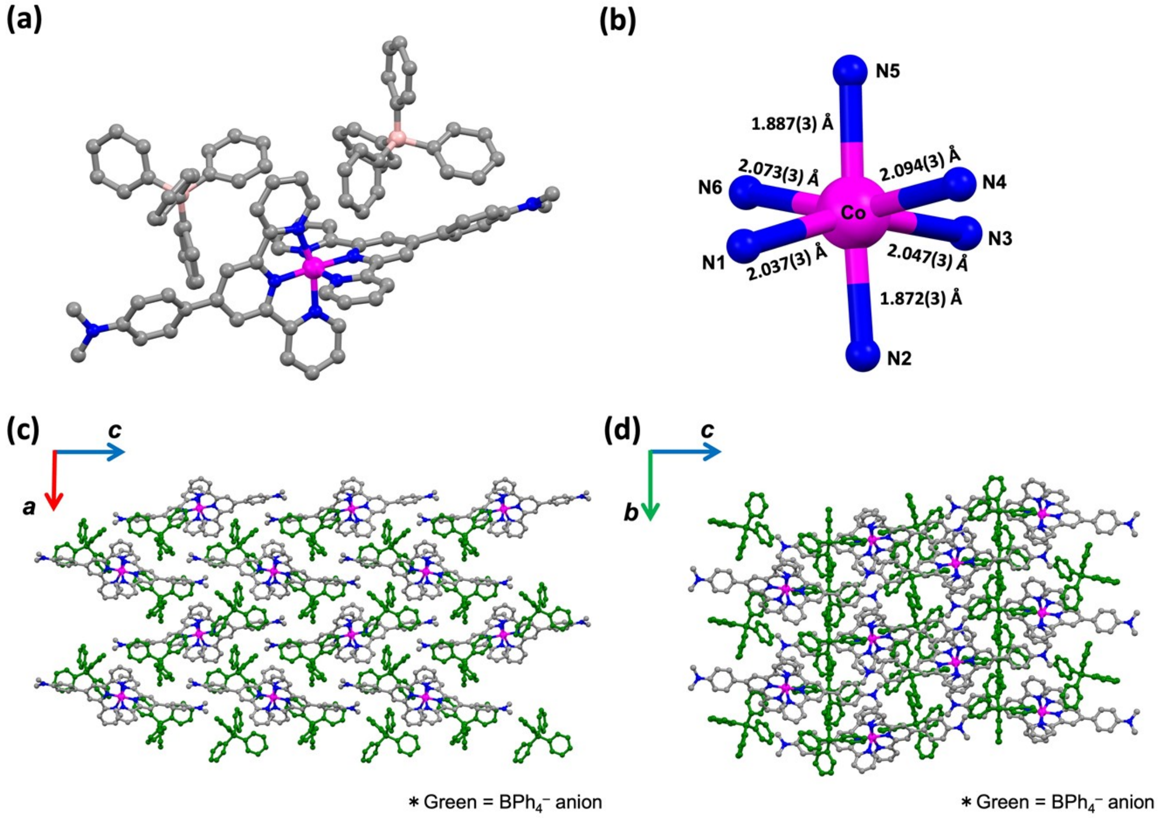

Fig. S6 (a) Crystal structure of **2·BPh$_4$**. H atoms are omitted for the clarity. (b) Coordination environment of the [CoN6] core and the Co–N bond length. Crystal packing of **2·BPh$_4$** along (c) the *ab* plane and (d) the *bc* plane.

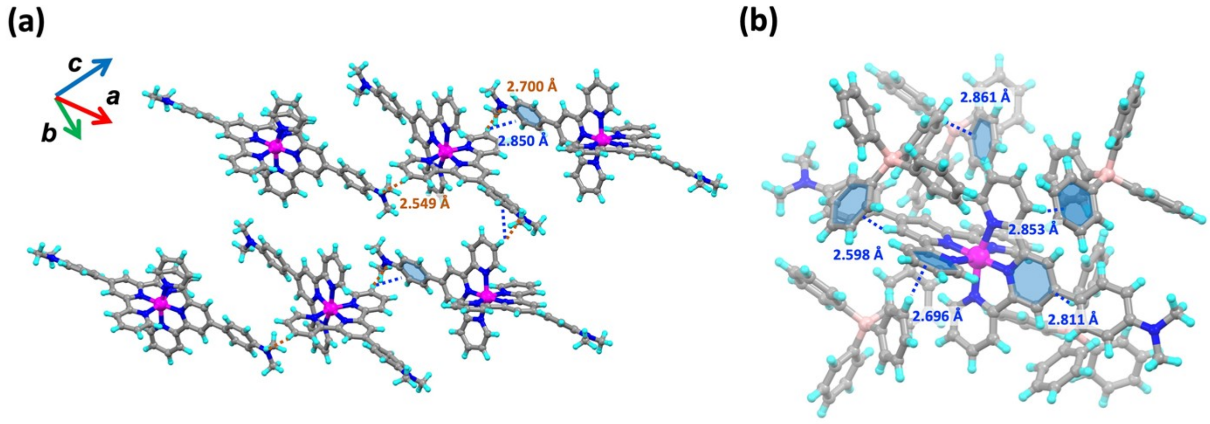

Fig. S7 The selected intermolecular interactions observed in the molecular assembly of **2·BPh$_4$**. (a) Illustration of intermolecular N···H interactions (orange dashed line) and CH–π interactions (blue dashed line), respectively, among the [Co(**L2**)]$^{2+}$ units. BPh$_4^-$ counter anions are omitted for clarity. (b) Intermolecular CH–π interactions among a [Co(**L2**)]$^{2+}$ unit and BPh$_4^-$ counter anions (blue dashed line).

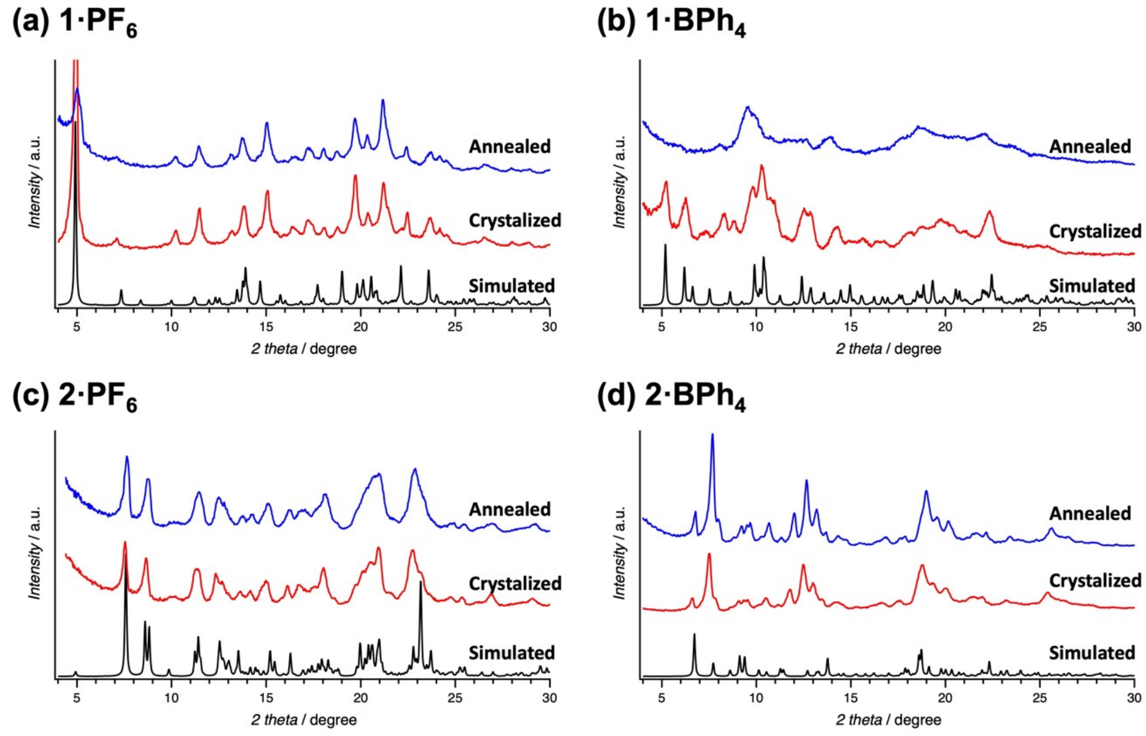

Fig. S8 PXRD patterns for (a) **1·PF$_6$**, (b) **1·BPh$_4$·3CH$_3$CN·MeOH**, (c) **2·PF$_6$** and (d) **2·BPh$_4$**. Black solid line indicates the patterns simulated from the SC-XRD data. Red solid lines are experimentally obtained from the recrystalized samples. Blue solid lines indicate the annealed samples at 100 °C in vacuo.

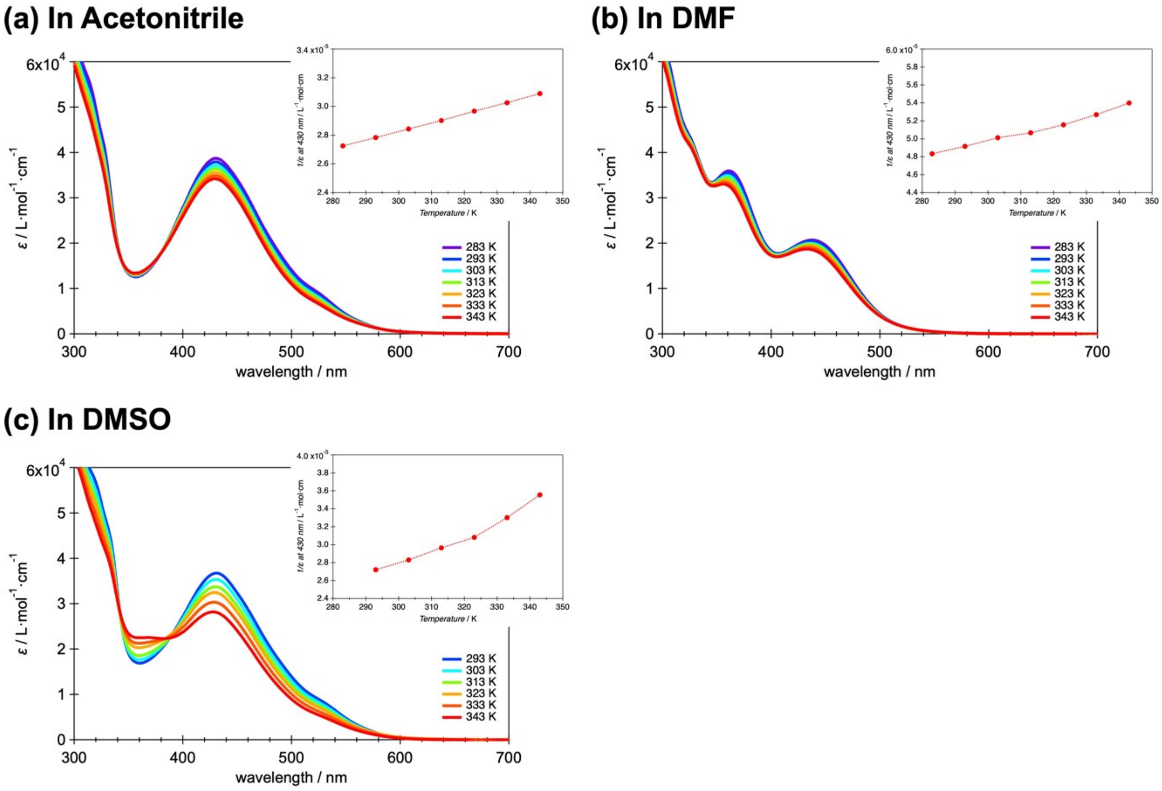

Fig. S9 Effect of temperature on the molar adsorption constant (ε) of $\mathbf{1{\cdot}PF_6}$ in (a) acetonitrile, (b) DMF and (c) DMSO. The temperature was varied from 283 – 343 K except for trials with DMSO, which used 293 – 343 K due to the higher freezing point of this solvent. The insets show plots of *T* vs $1/\varepsilon$.

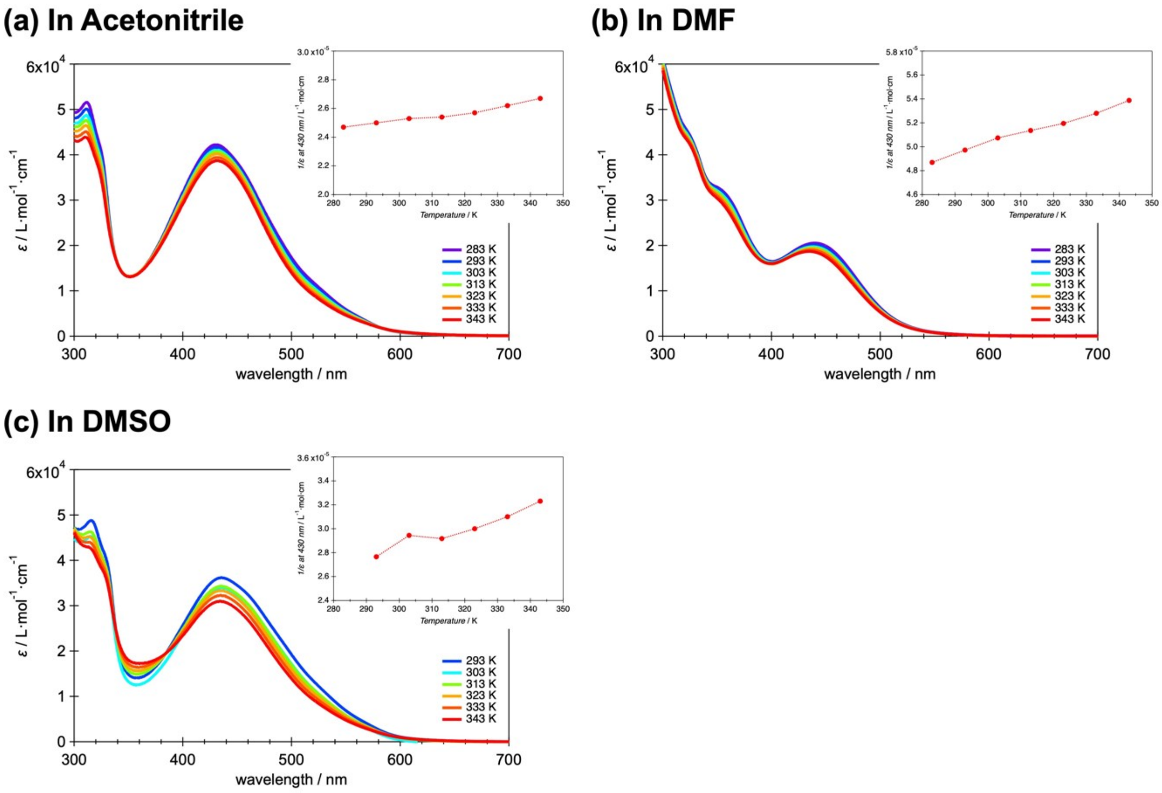

Fig. S10 Effect of temperature on the molar adsorption constant (ε) of **2·PF$_6$** in (a) acetonitrile, (b) DMF and (c) DMSO. The temperature was varied from 283 – 343 K except for trials with DMSO, which used 293 – 343 K due to the higher freezing point of this solvent. The insets show plots of *T* vs $1/\varepsilon$.

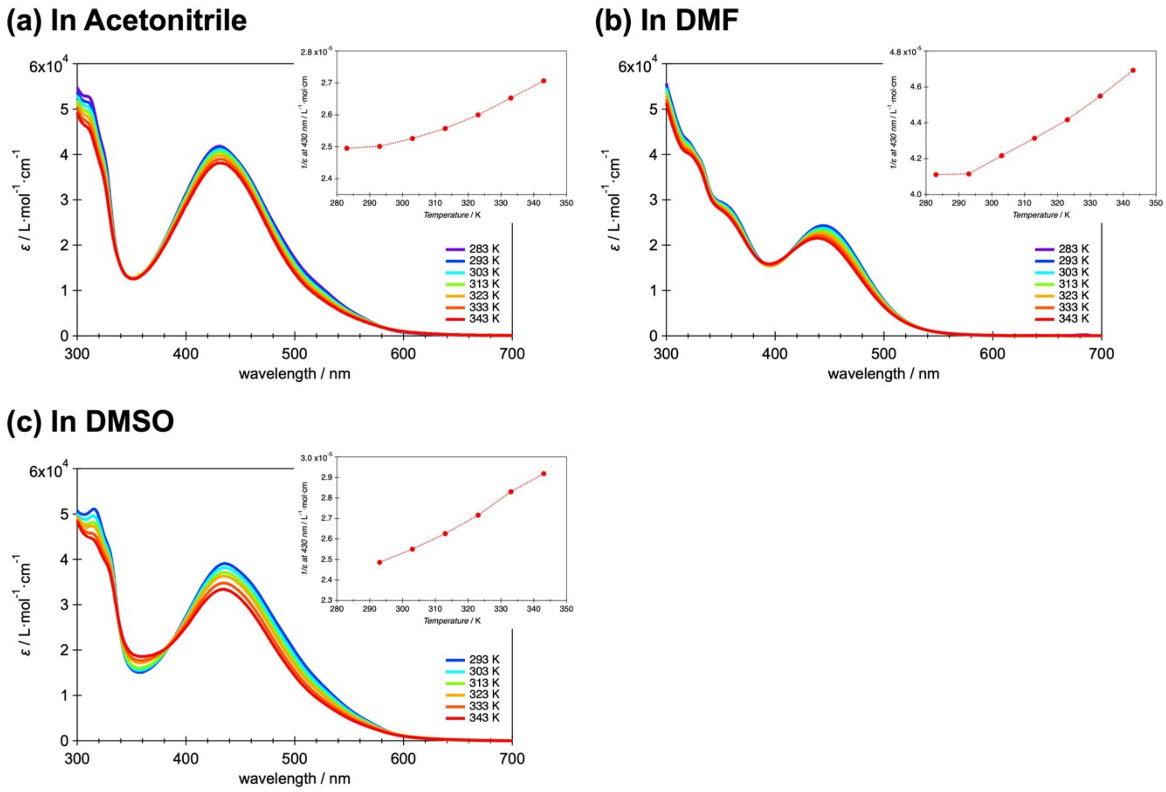

Fig. S11 Effect of temperature on the molar adsorption constant (ε) of **2·BPh$_4$** in (a) acetonitrile, (b) DMF and (c) DMSO. The temperature was varied from 283 – 343 K except for trials with DMSO, which used 293 – 343 K due to the higher freezing point of this solvent. The insets show plots of T vs $1/\varepsilon$.

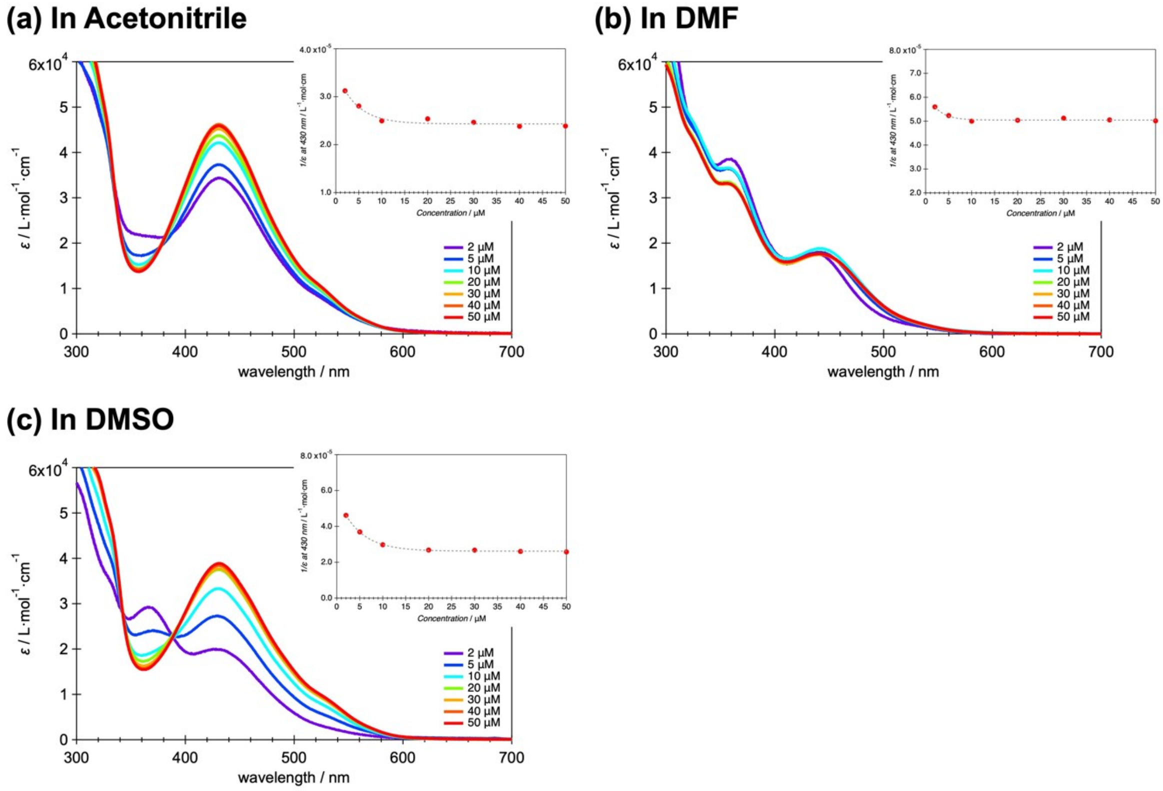

Fig. S12 Effect of concentration on the molar adsorption constant (ε) of **1·PF$_6$** in (a) acetonitrile, (b) DMF and (c) DMSO. The complex concentration was varied from 2 – 50 µM. The insets show plots of 1/ε versus T.

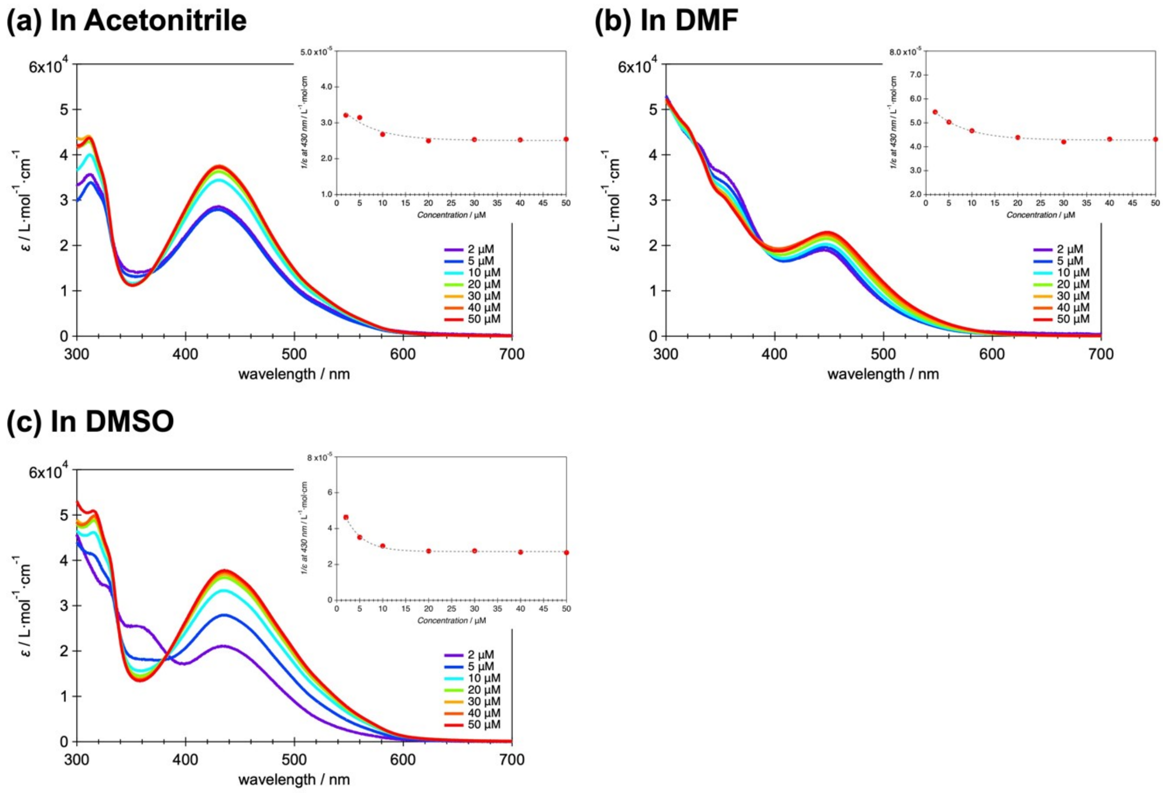

Fig. S13 Effect of concentration on the molar adsorption constant (ε) of **2·PF_6** in (a) acetonitrile, (b) DMF and (c) DMSO. The complex concentration was varied from 2 – 50 μM. The insets show plots of $1/\varepsilon$ versus T.

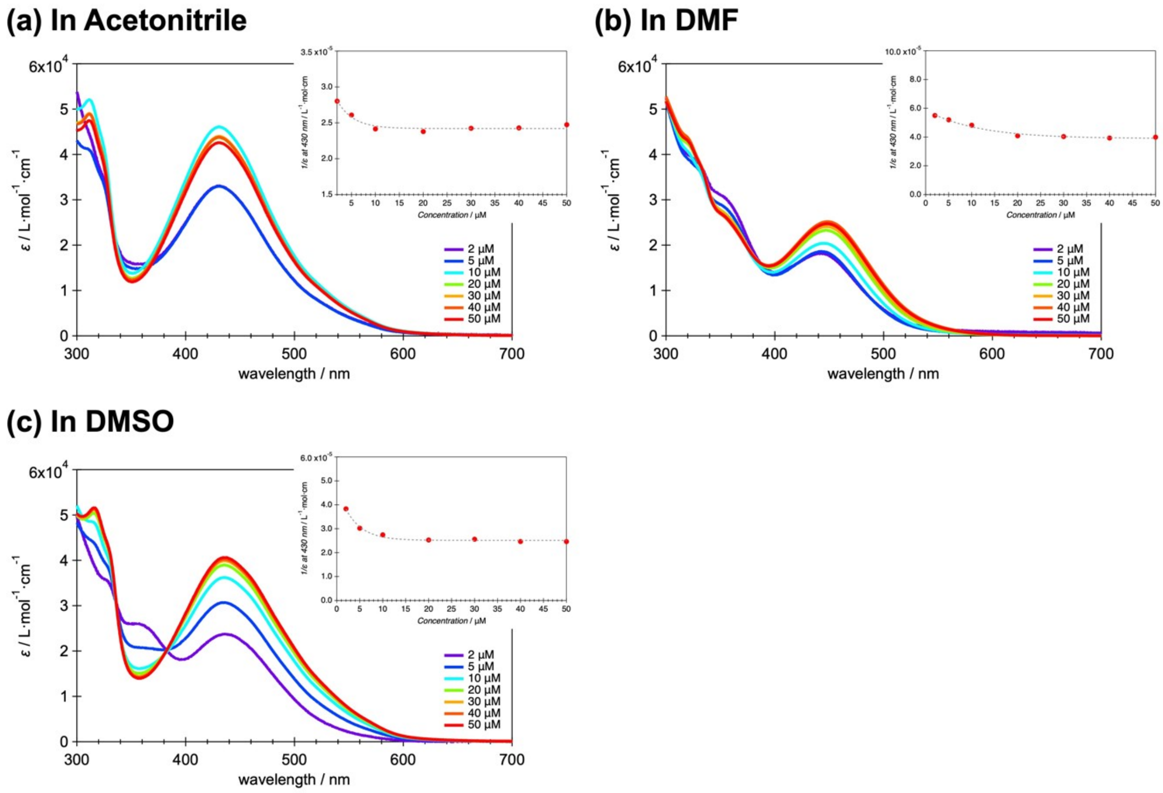

Fig. S14 Effect of concentration on the molar adsorption constant (ε) of **2·BPh$_4$** in (a) acetonitrile, (b) DMF and (c) DMSO. The complex concentration was varied from 2 – 50 μM. The insets show plots of 1/ε versus T.